

Research Article

Parameter Study of GTN Model in a SLM Manufactured Lattice Structure under Compression by Using FEM

M. Araghi¹, A. Nayebi^{1*} and H. Rokhgireh²¹ Department of Mechanical Engineering, Shiraz University, Shiraz, Iran² Department of Mechanical Engineering, University of Larestan, Lar, Iran

ARTICLE INFO

Article history:

Received 19 January 2020

Revised 7 August 2020

Accepted 4 October 2020

Keywords:

Parameter Study

GTN model

Isotropic hardening

SLM

ABSTRACT

This study investigates the effect of material parameters of the Gurson-Tvergaard-Needleman (GTN) model on the failure prediction of cellular structures. The effect of elastic modulus, calibration parameter of GTN model, isotropic hardening, fracture strain, and strut diameter on the load-displacement curve of a lattice structure fabricated by Selective Laser Melting (SLM) has been studied by using the finite element method. The power law of Hollomon has been used to model the isotropic hardening behavior. The considered lattice structure is made of AlSi10Mg alloy, which is used in different industries. A 20cm×20cm×20cm structure with 4 Body Centered Cubic (BCC) unit cells in x, y, and z directions have been considered. The results show that 250000 elements for one-quarter of the lattice structure are quite enough to obtain acceptable results. The effect of prescribed parameters on the load-displacement curve of the lattice structure has been studied. Based on the obtained results, diameter and hardening behavior are the most influential parameters and the significant effect on load-displacement curve has been observed.

© Shiraz University, Shiraz, Iran, 2020

1. Introduction

Additive manufacturing methods are used to produce optimum structures with high strength to weight ratio and they are the engineering solution to the real life applications in aerospace, automotive, and many other industries. In this context, lattice structures could be very useful. Among different methods for producing these structures, SLM has attracted a lot of attention. This method offers excellent degree of freedom in manufacturing. However, SLM manufactured parts have voids, pores, and unmelted powders which act as stress concentration zones [1]. Local yielding occurs at these sites and plastic flow begins [4].

The existence of voids and their growth affects the yield behavior of the material and has been studied by many researchers. Basic studies in this field has been performed by McClintock [2], Rice and Tracey [3], and Gurson [4]. Gurson proposed a model that incorporates the effect of material porosity to the yield behavior of metals [5]. Tvergaard introduced three calibration parameters q_1 , q_2 , and q_3 into the Gurson yield criterion to obtain better agreement with the numerical simulations of a voided material [6]. Tvergaard and Needleman extended the Gurson-Tvergaard model to include coalescence by modifying the void volume fraction [7].

* Corresponding author

E-mail address: nayebi@shirazu.ac.ir (A. Nayebi)

Amani et al. [8] studied the effect of strut diameter and node radius in compressive test of a lattice structure. They simulated the compression test by using the GTN model and assumed that the porosity distribution is homogenous and heterogeneous. Their result showed that heterogeneous model is in agreement with the experimental results. Leary et al. [9] investigated the mechanical properties and manufacturability of different types of lattice structures of AlSi10Mg fabricated by SLM through experiment and numerical modeling. The effect of layer and cell numbers on quasi-static response of different types of lattice structure fabricated by SLM has been investigated by Li et al. [10]. Their results showed that layer-by-layer progressive damage is the main failure mode in the multi-layer lattice structure.

Irmak and Troster [11] investigated the tensile test of specimens fabricated by SLM with 0°, 45° and 90° scan direction. Their results showed that larger pores in structures are critical and numerical results revealed that the existence of randomly distributed pores in the model made more realistic description of the material behavior. Costas et al. [12] showed that under quasi-static loading conditions, 3D finite element models could predict the structural response of the additively manufactured parts. Samei et al. [13] experimentally showed that significant pore coalescence occurs at the final stage of tensile test of additively manufactured specimen made by AlSi10Mg indicating ductile failure.

Delroisse et al. [14] investigated the pores in inclined and vertical struts of AlSi10Mg and found that vertical struts were fully dense with a homogenous microstructure; while, inclined struts exhibited large pores and a heterogeneous microstructure. Dong et al. [15] investigated the influence of built size on porosity content in AlSi10Mg alloys. They reported that porosity volume fraction increased significantly with the decrease in built size.

Kempen et al. [16] showed that AlSi10Mg parts produced by SLM have mechanical properties higher or at least comparable to the cast material because of their

very fine microstructure. Chen et al. [17] studied the mechanical properties, porosity and microstructure of AlSi10Mg alloy produced by SLM by using Finite element analysis and experiments. According to their results, there were no obvious distinctions in the strength between the transverse and longitudinal directions. Liu et al. [18] investigated the growth and orientation of microstructures in the node and struts of BCC lattice structures. According to their results, gradient microstructure was observed at the nodes. In addition, it must be noted that the orientation of the microstructures in the struts aligned to the direction of the struts further qualify the anisotropic growth of the microstructures.

2. Problem Explanation, Innovations and Aims of Paper

The objective of this study is to perform a parameter study of GTN plasticity model for the compression of lattice structures made by SLM. Effect of porosity, elastic Modulus, yield stress, calibration parameters (q_1 , q_2 , and q_3) of the GTN yield function, material hardening, fracture strain, and diameter of struts on the mechanical response of the lattice structure have also been investigated.

3. GTN Failure Model

The GTN model is developed based on von Mises yield criteria of ductile porous materials incorporating void nucleation and growth. This model can capture the main features of the void nucleation and growth and has fewer model constants with respect to the recent models. The GTN yield function is depicted as follows [7]:

$$\frac{\Sigma_{eq}^2}{\bar{\sigma}^2} + 2f^* q_1 \cosh \left(q_2 \frac{3 \Sigma_{hyd}}{2 \bar{\sigma}} \right) - 1 - q_3 f^{*2} = 0 \quad (1)$$

where $\bar{\sigma}$ is the flow stress of the matrix material. Σ_{eq} and Σ_{hyd} are effective macroscopic von Mises and hydrostatic stress, respectively. This model will reduce to Gurson's model by setting $q_1=q_2=q_3=1$. The effective porosity, f^* , is calculated by Eq. (2) [7].

$$f^* = \begin{cases} f & f \leq f_c \\ f_c + \frac{f_u^* - f}{f_f - f_c} (f - f_c) & f \geq f_c \end{cases} \quad (2)$$

f_c is the critical porosity, f_u^* is the ultimate porosity, and f_f is the porosity at fracture. The porosity fraction increment df^* is the sum of the nucleation porosity fraction, $df_{Nucleation}$ and the growth porosity fraction, df_{growth} . These porosity increments can be obtained as follows [7]:

$$df_{Nucleation} = \frac{f_N}{S_N \sqrt{2\pi}} \exp\left(-\frac{1}{2} \left(\frac{\varepsilon_p - \varepsilon_N}{S_N}\right)^2\right) d\varepsilon_p \quad (3)$$

and

$$df_{growth} = (1 - f) d\varepsilon_p^{ii} \quad (4)$$

f_N is the void volume fraction of the nucleated void; ε_N is the mean value of the normal distribution of the nucleation strain; and S_N is the standard deviation. ε_p^{ii} is the trace of the plastic strain tensor. A power law has been used to model the isotropic hardening behavior, which is known as Hollomon's law:

$$\sigma = k \varepsilon_p^n \quad (5)$$

In Eq. (3), ε_p is the plastic strain, k and n are the strength coefficient and the hardening exponent, respectively.

To investigate the effect of mesh dependency on the numerical results, the convergence of the load-displacement has been studied. It is known that material properties of SLM parts are dependent on many factors like scan speed, scan strategy, build direction, hatch distance, and laser power during manufacturing process [1], such that different values for elastic modulus, yield stress, and hardening behavior has been reported. Table 1 depicts the used values for the model parameters and mechanical properties. Different experiments proved that the yield stress of the AlSi10Mg part produced by SLM is about 200 MPa [8, 12, 13, 16]. The elastic modulus also changes from 40 to 70 MPa as stated by many references [8, 12]. The initial porosity of SLM manufactured parts depends on different manufacturing parameters and it is varied according to [1, 8, 12].

Table 1. Used material constants to perform parameter study

E (GPa)	40		70	
σ_y (MPa)	200			
n	0.0	0.05	0.1	0.15
q_1	1		1.5	
q_2	1			
$q_3 = q_1^2$	1		2.25	
f_0	0.01		0.02	

4. Numerical Modelling and Validation

In order to compare FEM results with the experimental results of [8], one-quarter of a 20cm×20cm×20cm BCC lattice structure with 4 unit cells in x, y, and z directions (Fig. 1), is modeled in CAD software and imported to ABAQUS/CAE. The strut diameters are 0.8 mm and 1 mm with a core fillet radius of 0.25 mm.

To simulate the compression test of the lattice structure, the bottom surface is constrained in the compression direction. This surface is free to elongate in the x and z directions. Two symmetry conditions are considered in the simulation due to the symmetric geometry and boundary conditions. The top surface of the lattice structure is displaced -5 mm in the y direction. Other surfaces are stress free. C3D8 elements are used in these simulations. Fig. 1 illustrates the geometry and boundary conditions used in the simulation.

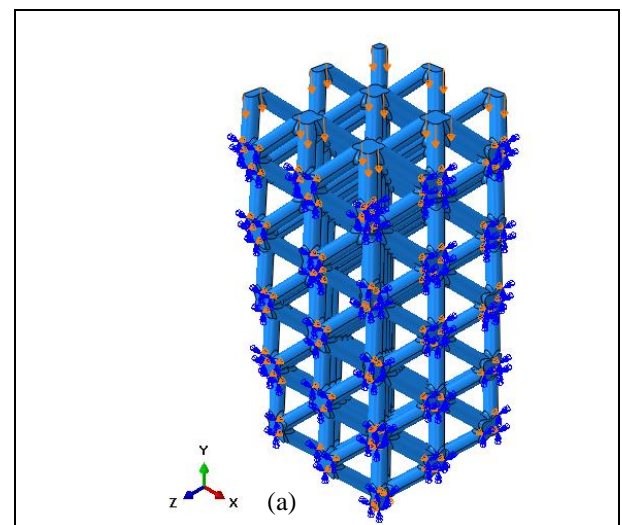


Fig. 1. a) geometry and b) boundary conditions of the cellular structure.

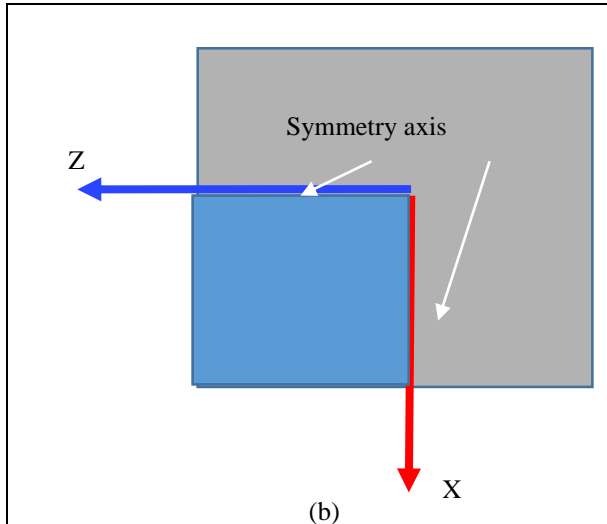


Fig. 1. Continue.

In order to verify the numerical results, a thin strut model presented by Amani et al. [8] has been prepared. Fig. 2 illustrates the obtained FEM results of the compression test. The results are in agreement with the experimental results of [8]. According to Fig. 2, GTN model does not underestimate stress-strain curve compared to the experimental results. Besides, in the plastic deformation region, the obtained results are close to the experimental results in comparison with the results of Amani et al. [8]. The following relations have been used to obtain the equivalent stress and strain in Fig. 2.

$$\text{equivalent stress} = \frac{\text{total force}}{\text{total cross sectional area}} = \frac{\text{total force}(N)}{20(mm) \times 20(mm)} \quad (6)$$

$$\text{strain} = \frac{\text{change of length}}{\text{height}} = \frac{\text{change of length}(mm)}{20(mm)} \quad (7)$$

5. Results and Discussions

In order to carry out the mesh analysis, the structure is modeled with 61000, 150251, 251146, 450087, and 646300 elements and the effect of mesh dependency on load-displacement curve is studied. Fig. 3 shows the numerical results of load-displacement curve of a 1 mm and 0.8 mm strut diameter for the above mentioned element numbers.

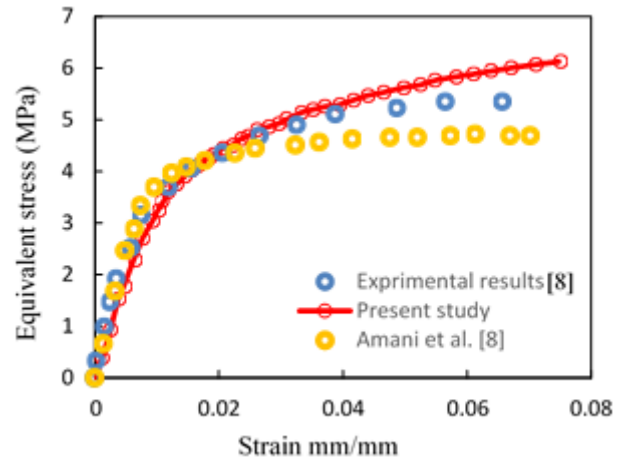


Fig. 2. Comparison of the numerical results with constants of Amani et al. [8], experimental result, and results of Amani et al. [8].

The convergence answers of the lattice structure with different hardening exponents are demonstrated in Figs. 4-6. Similar results were obtained for other simulated cases. It can be seen that when the number of the elements are about 250000, the increase of the number of the elements does not change the numerical applied load-displacement results and the difference between the maximum applied load is less than 3%. According to the above results, the mesh of the lattice structure with about 250000 elements is satisfactory.

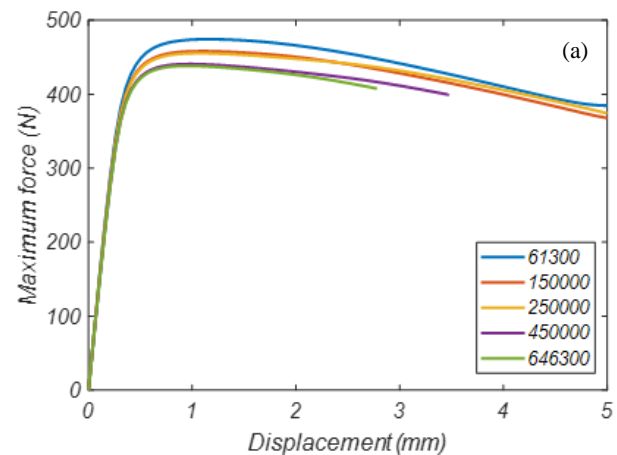


Fig. 3. Maximum load-displacement curves of the cellular structure of a) 1 mm and b) 0.8 mm strut diameter with perfect plastic behavior.

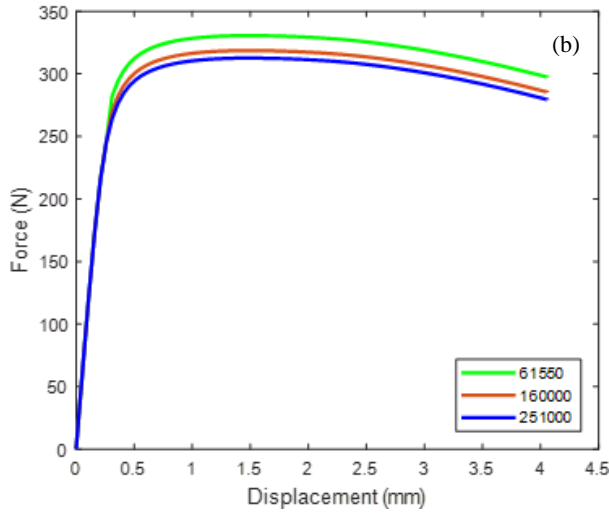


Fig. 3. Continue.

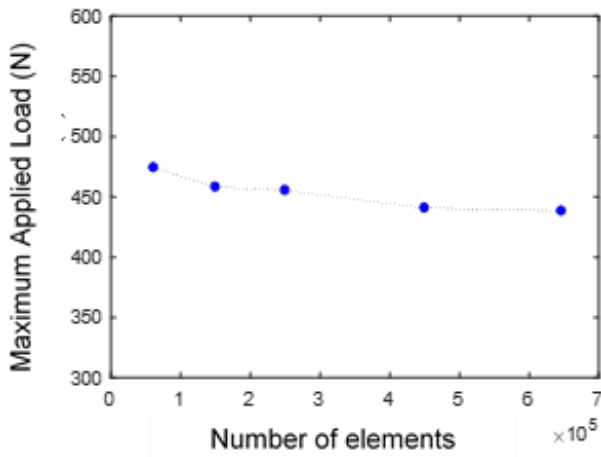


Fig. 4. Convergence of the maximum applied load for 1 mm strut lattice structure with perfect plastic behavior.

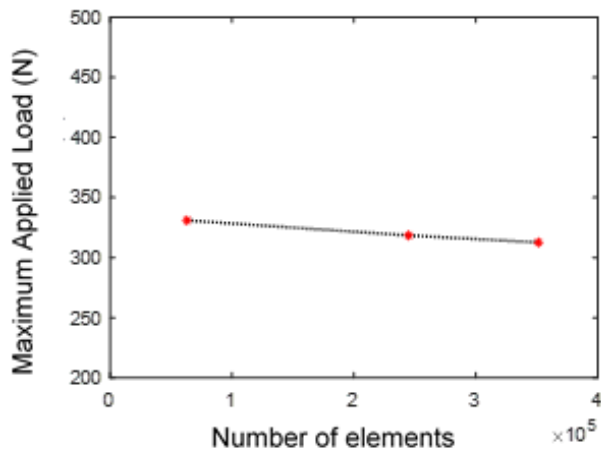


Fig. 5. Convergence answer of the lattice structure of 0.8 mm strut diameter and the hardening exponent of 0.05.

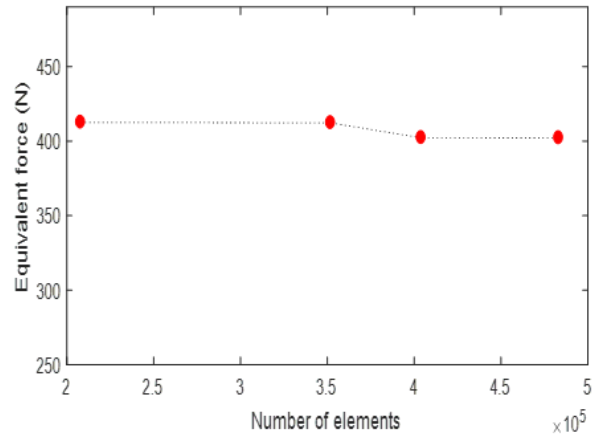


Fig. 6. Convergence answer of the lattice structure of 0.8 mm strut diameter and the hardening exponent of 0.15.

The first set of material constants to be investigated are the calibration parameters and the initial porosity. Figs. 7 and 8 show the applied load- displacement curves for Gurson’s model with $q_1=q_2=q_3=1$ and GTN model with $q_1=1.5$, $q_2=1$, and $q_3=2.25$ for elastic modulus of 40 GPa and 70 GPa, respectively. The initial porosity is considered to be 0.01 and 0.02 for the above mentioned cases, respectively. According to Fig. 7 and Fig. 8, increasing calibration parameters has a detrimental effect on the loading capacity of the structure. This effect is due to the consideration of the growth and coalescence of voids in the GTN model with respect to Gurson’s model. Therefore, the voids and porosity ratio increases more rapidly for the GTN model than it does for Gurson’s model.

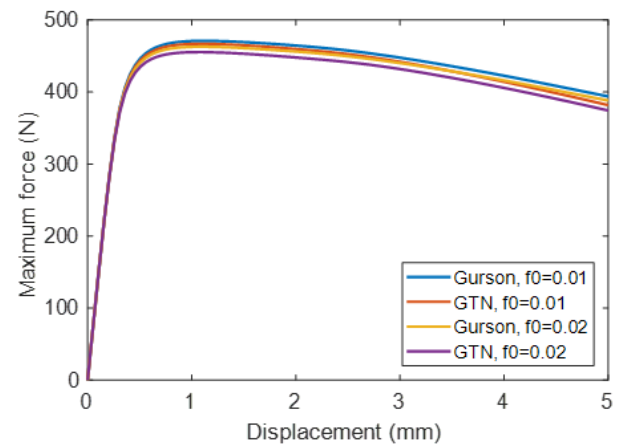


Fig. 7. Maximum load-displacement curve of the cellular structure of $E = 40$ GPa.

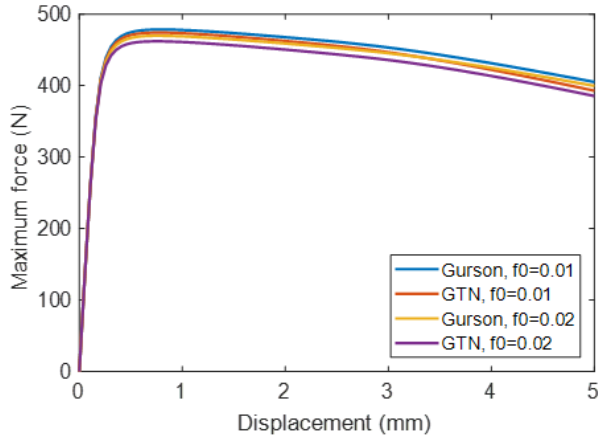


Fig. 8. Maximum load-displacement curve of the cellular structure of E = 70 GPa.

Both structures, with different elastic modulus, show similar effect of the initial porosity. When the initial porosity increases the needed applied load decreases for the same displacement. The difference between maximum applied load for elastic moduli of 70 GPa are about 15.37 N and 17.47 N which yield about 3.1 percent decrease of maximum load for both cases, respectively.

The effect of each parameter on numerical results can be represented separately. Maximum applied load versus initial porosity and calibration parameters are plotted in Fig. 9 and Fig. 10, respectively. The initial porosity is related to the manufacturing method of SLM due to the unmelted powders, trapped gases, etc. The influence of the initial porosity on the load capacity of the structure, is very important. Increase of the initial porosity means that the effective area decreases leading to a fall in the needed load for the same displacement.

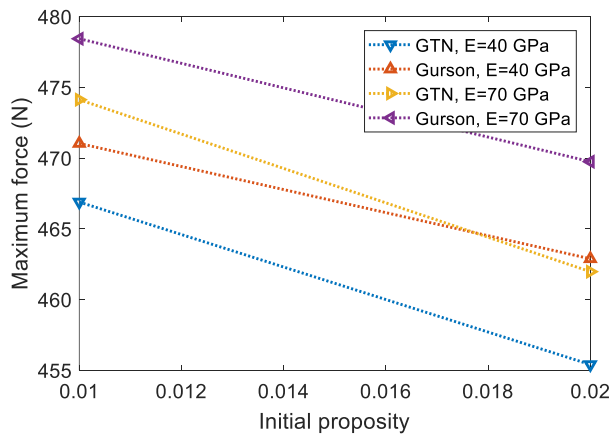


Fig. 9. Effect of the initial porosity on the maximum load for both the GTN and Gurson's models and both elastic constants.

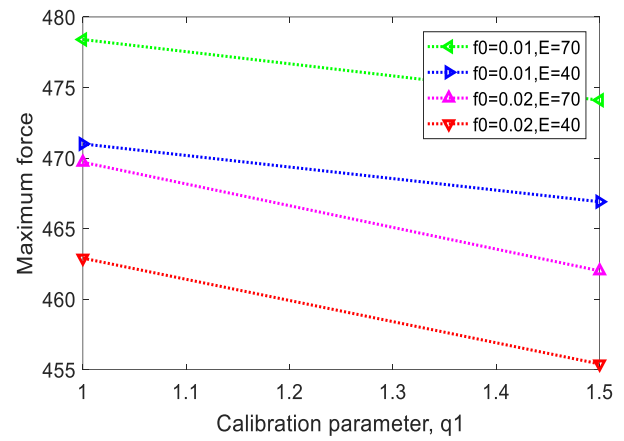


Fig. 10. Effect of the first calibration parameter, q_1 .

From the above data we can see that initial porosity and calibration parameters will have more significant effects on the model with higher elastic modulus., It can be also concluded from Fig. 10 that for initial porosities larger than 0.0178, the maximum load of the GTN model with E = 70 GPa is lower than the maximum load of Gurson's Model with E = 40 GPa.

Another considered parameter for material dependency analysis is fracture strain, ϵ_n . Fig. 11 shows the effect of this parameter on load-displacement curve. As can be seen in Fig. 11, the fracture strain parameter has little effect on the maximum applied load and only controls the rate of material degradation. The first row of Table 2 shows the combination that is typically used for the void nucleation option in ABAQUS/CAE and typically used by researchers [5]. The other rows are considered here to investigate the effect of this parameter.

Table 2. Material parameters of void nucleation by the GTN model

s_n	ϵ_n	f_n
0.18	0.06	0.04
0.1	0.1	0.04
0.1	0.2	0.04
0.1	0.3	0.04

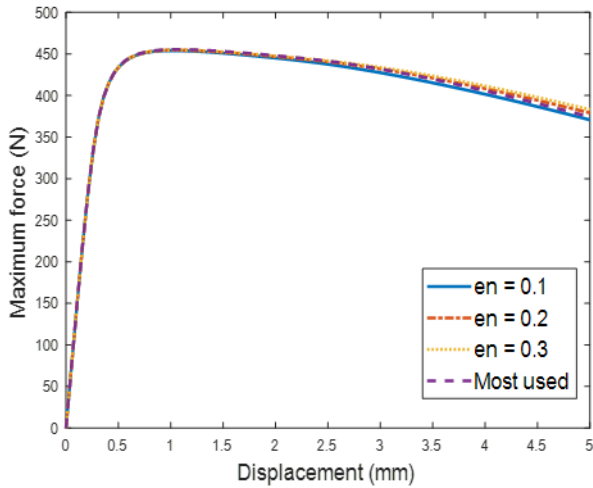


Fig. 11. Effect of fracture strain on maximum applied load-displacement curve.

The effects of hardening exponent on the applied load-displacement curve is investigated and four values of hardening exponents are: 0, 0.05, 0.1, and 0.15. As can be seen in Fig. 12, an increase in the hardening exponent shifts the maximum applied load to the higher value of the displacement. Figs. 13 and 14 illustrate the effect of the hardening exponent on the maximum applied load and the displacement corresponding to this load for two initial porosity values. When the hardening exponents increases, the effect of strain hardening becomes more important and the necessary load for the same displacement increases. Moreover, the plastic strain decreases for the same stress, by increasing the hardening exponent and so the nucleation and growth rates of the voids decrease. This leads to a shift of the failure to higher displacements.

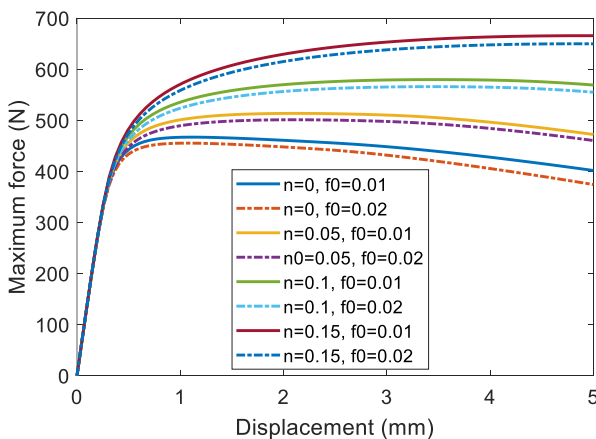


Fig. 12. Effect of hardening exponent on the maximum load-displacement curve.

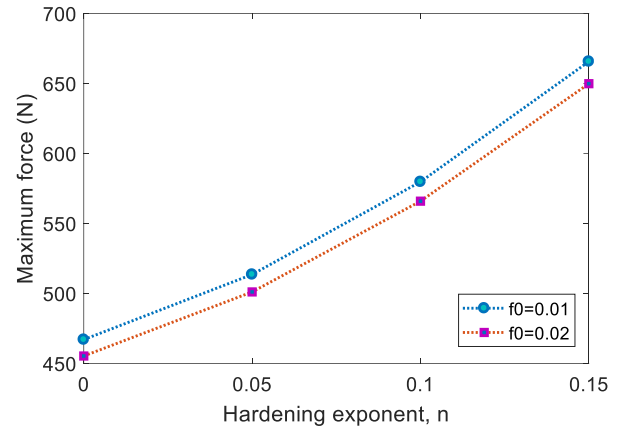


Fig. 13. Effect of hardening exponent on the maximum applied load.

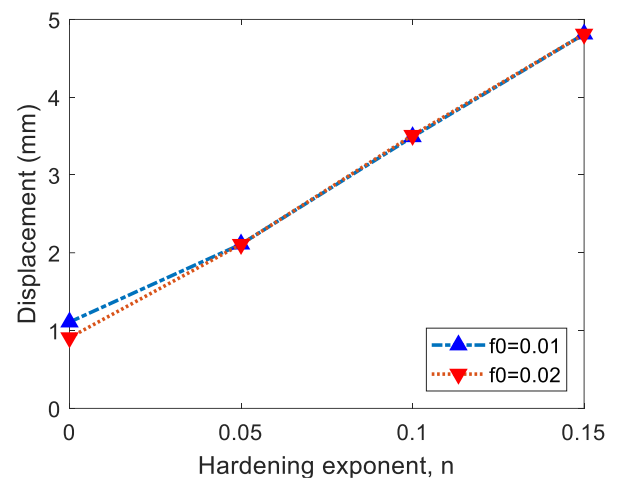


Fig. 14. Effect of hardening exponent on the displacement corresponding to the maximum load.

It has been also observed that the applied load on the lattice structures made by SLM depends on the diameter of the struts. So, it's reasonable to perform a dependency analysis to the diameter. The maximum applied load for a strut diameter of 1 mm diameter is about 455 N (Fig. 1(a)) and it is 312 N (Fig.1(b)) for 0.8 mm strut diameter, when the perfect plasticity model is considered. It means that a 25 percent increase of diameter leads to a 31.43 percent increase of the maximum applied load. If the hardening exponent is 0.15, the load increase is about 39.85 percent (Figs. 6 and 12). This behavior could help us in designing and manufacturing lattice structures with optimum strength to weight ratio. The effect of strut diameter is much more important than the other parameters such as initial porosity or void growth constants.

6. Conclusions

The effect of the GTN failure model on the applied load-displacement of a cellular structure under compression, is studied in this research. The finite element method has been used by performing the mesh analysis. The obtained FEM results have been compared with the numerical and experimental results of Amani et al. [8] who studied the same lattice structure. Initial porosity and calibration parameters similarly impacts the maximum load-displacement as well as the applied load-displacement curve. Calibration parameters incorporate the effect of the shape of the voids and their interactions in the model while the initial porosity represents the volume fraction of the voids to the volume of the homogenized representative volume elements.

Fracture strain has little effect on the maximum load. Hardening behavior is studied by varying the hardening exponent. Increase of the hardening exponent from 0 to 0.15, increases the maximum load of about 30 percent for both initial porosities. The change of the maximum load with the hardening exponent has a nonlinear behavior while the displacement corresponding to the maximum load shows almost a linear change for hardening power greater than 0.05. Another parameter, which shows a significant effect on the maximum load-displacement curve, is diameter of the struts. The effect of this parameter is in the order of the hardening exponent.

7. References

- [1] T. DebRoy, H.L. Wei, J.S. Zuback, T. Mukherjee, J.W. Elmer, J.O. Milewski, W.T. Zhang, Additive manufacturing of metallic components-Process, structure and properties, *Progress in Materials Science*, 92 (2018) 112-224.
- [2] F. A. McClintock, A Criterion for Ductile Fracture, *Journal of Applied Mechanics*, 35(2) (1968) 363-371.
- [3] J.R. Rice, D. M. Tracy, On the ductile enlargement of voids in triaxial stress fields, *Journal of the Mechanics and the Physics of the Solids*, 17(3) (1969) 201-217.
- [4] Z. Chen, C. Butcher, Micromechanics Modelling of Ductile Fracture, Springer, London (2013).
- [5] A.L. Gurson, Continuum Theory of Ductile Rupture by Void Nucleation and Growth: Part 1- Yield Criteria and Flow Rules for Porous Ductile Media, *Journal of Engineering Materials and Technology*, 92(1) (1977) 2-15.
- [6] V. Tvregaard, Influence of voids on shear band instabilities under plane strain conditions, *International Journal of Fracture*, 17 (4) (1981) 389-407.
- [7] V. Tvregaard, A. Needleman, Effects of nonlocal damage in porous plastic solids, *International Journal of Solids and Structures*, 39 (8) (1984) 1063-11077.
- [8] Y. Amani, S. Dancette, P. Delroisse, A. Simar, E. Maire, Compression of lattice structures produced by selective laser melting: X-ray tomography based experimental and finite element approaches, *Acta Materialia*, 159 (2018) 395-407.
- [9] M. Leary, M. Mazur, J. Elambasseril, M. McMillan, T. Chirent, Y. Suna, M. Qian, M. Eastona, M. Brandt, Selective laser melting (SLM) of AlSi12Mg lattice structures, *Materials and Design*, 98 (2016) 344-357.
- [10] C. Li, H. Lei, Y. Liu, X. Zhang, J. Xiong, H. Zhou, D. Fang, Crushing behavior of multi-layer metal lattice panel fabricated by selective laser melting, *International Journal of Mechanical Sciences*, 145 (2018) 389-399.
- [11] E.F.A. Irmak, T. Troster, T., 2019. "Fracture prediction of additively manufactured AlSi10Mg materials, *Procedia Structural Integrity*, 21 (2019) 190-197.
- [12] M. Costas, D. Morin, M. de Lucio, M. Langseth, Testing and simulation of additively manufactured AlSi10Mg components under quasi-static loading, *European Journal of Mechanics / A Solids*, 81 (2020) 103966.
- [13] J. Samei, M. Amirmaleki, M. Shirinzadeh Dastgiri, C.E. Marinelli, D.E. Green, In-situ X-ray tomography analysis of the evolution of pores during deformation of AlSi10Mg fabricated by selective laser melting, *Materials Letters*, 255 (2018) 126512.
- [14] P. Delroisse, P.J. Jacques, E. Maire, O. Rigo, A. Simar, Effect of strut orientation on the microstructure heterogeneities in AlSi10Mg lattices processed by selective laser melting, *Scripta Materialia*, 141 (2017) 32-35.
- [15] Z. Dong, X. Zhang, W. Shi, H. Zhou, H. Lei, J. Liang, Study of size effect on microstructure and mechanical properties of

- AlSi10Mg samples made by selective laser melting, *Materials (Basel)* (2018), 11.
- [16] K. Kempen, L. Thijs, J. Van Humbeeck, J.P. Kruth, Processing AlSi10Mg by selective laser melting: parameter optimization and material characterization, *Materials Science and Technology*, 31 (8) (2015) 917-923.
- [17] L. Jing Chen, W. Hou, X. Wang, S. Chu, Z. Yang, Microstructure, porosity and mechanical properties of selective laser melted AlSi10Mg, *Chinese Journal of Aeronautics*, 33(7) (2020) 2043-2054.
- [18] M. Liu, N. Takata, A. Suzuki, M. Kobashi, Development of gradient microstructure in the lattice structure of AlSi10Mg alloy fabricated by selective laser melting, *Journal of Materials Science and Technology*, 36 (2019) 106-117.

مطالعه اثر پارامترهای مدل GTN برای بارگذاری فشاری یک سازه شبکه ای تولید شده توسط SLM به کمک روش اجزاء محدود

مهران عراقی^۱، علی نایبی^۱ و حجت الله رخ گیره^۲

۱- دانشکده مهندسی مکانیک، دانشگاه شیراز، شیراز، ایران.

۲- دانشکده مهندسی مکانیک، مجتمع آموزش عالی لارستان، لار، ایران.

چکیده

این مطالعه به تأثیر پارامترهای مدل GTN (Gurson-Tvergaard-Needleman) در پیش بینی شکست ساختارهای سلولی می پردازد. اثر مدول الاستیک، پارامتر کالیبراسیون مدل GTN، سخت شوندگی همسانگرد، کرنش شکست و قطر میله ها در منحنی جابجایی-بار یک ساختار شبکه ای ساخته شده توسط روش ذوب انتخابی توسط لیزر (SLM)، توسط روش اجزای محدود بررسی شده است. از رابطه توانی Hollomon برای مدل سازی رفتار سخت شوندگی همسانگرد استفاده شده است. ساختار شبکه در نظر گرفته شده از آلیاژ AlSi10Mg ساخته شده که در صنایع مختلف استفاده می شود. یک ساختار $20\text{cm} \times 20\text{cm} \times 20\text{cm}$ با ۴ سلول BCC در جهت های x، y و z در نظر گرفته شده است. نتایج نشان می دهد که ۲۵۰۰۰۰ المان برای یک چهارم ساختار شبکه به منظور دستیابی به نتایج قابل قبول کاملاً کافی است. اثر پارامترهای انتخاب شده بر روی منحنی جابجایی-بار ساختار شبکه مورد مطالعه قرار گرفته است. بر اساس نتایج بدست آمده، قطر و رفتار سخت شدن از مهمترین پارامترها می باشند و آنها تغییر قابل توجهی بر منحنی جابجایی-بار ایجاد می کنند.

واژه های کلیدی: مطالعه پارامتریک، مدل GTN، سخت شوندگی همسانگرد، SLM